OPTIMIZATION OF THE REINFORCEMENT OF POLYMER-BASED NANOCOMPOSITES WITH GRAPHENE

L. Gong[1], R. J. Young[1]*, I. A. Kinloch[1], I. Riaz[2], R. Jalil[2], K. S. Novoselov[2]

[1]*School of Materials, University of Manchester, Oxford Road, Manchester M13 9PL, UK*
[2]*School of Physics and Astronomy, University of Manchester, Oxford Road, Manchester M13 9PL, UK*
** robert.young@manchester.ac.uk*

Keywords: Graphene, nanocomposites, mechanics, Raman spectroscopy.

Abstract
The stress transfer between the internal layers of multilayer graphene within polymer-based nanocomposites has been investigated from the stress-induced shifts of the 2D Raman band. This has been undertaken through the study of the deformation of an ideal composite system where the graphene flakes were placed upon the surface of a polymer beam and then coated with an epoxy polymer. It is found that the rate of band shift per unit strain for a monolayer graphene flake is virtually independent of whether it has one or two polymer interfaces (i.e. with or without an epoxy top coating). In contrast, the rate of band shift is lower for an uncoated bilayer specimen than a coated one, indicating relatively poor stress transfer between the graphene layers. Strain–induced Raman band shifts have also been evaluated for separate flakes of graphene with different numbers of layers and it is found that the band shift rate tends to decrease with an increase in the number of layers, indicating poor stress transfer between the inner graphene layers. Taking into account the packing geometry of polymer-based graphene nanocomposites and the need to accommodate the polymer coils, these findings enable the optimum number of layers for the best reinforcement to be found.

1 Introduction

Graphene is one of the most exciting topics in materials science and condensed matter physics [1] with good prospects for applications [2,3]. It was first isolated in Manchester in 2004 [4] and since that time the majority of the research effort has been concentrated upon investigating its electronic properties, aimed at using graphene in applications such as electronic devices [5]. The mechanical properties of graphene are also very promising with AFM nanoindentation of graphene layers finding a Young's modulus of the order of 1 TPa and an intrinsic strength of around 130 GPa [6]. These properties make it one of the stiffest and strongest materials ever measured and an ideal candidate for use as a reinforcement in high-performance composites. It is now established that Raman spectroscopy is one of the best methods of both characterizing graphene and following its subsequent deformation. Relatively strong, well-defined resonance Raman spectra are obtained even from single atomic graphene layers and the technique can be used to differentiate between monolayer, bilayer, trilayer and many-layer material, from the shape and position of the 2D (or G') Raman band [7]. It is also found that the positions of the Raman bands in graphene shift with stress [8,9] and that stress-induced Raman band shifts can consequently be employed to determine the stress in the material and so estimate its effective Young's modulus [8].

In recent papers [10,11] we have demonstrated unambiguously that stress transfer takes place from the polymer matrix to monolayer graphene, showing that the graphene has the capability of acting as a reinforcing phase in nanocomposites. This previous work has been undertaken through the use of model polymer nanocomposites in which monolayers of graphene were prepared by exfoliation and place upon a polymer beam with a thin layer of polymer spin-coated on the top to make a sandwich structure. Stress transfer from the polymer matrix to the graphene was monitored from the shift of the 2D Raman band. It was demonstrated, by following the variation of strain in the graphene across a flake, that at low strains continuum mechanics could be applied to this nanocomposite system [10] and the behavior could be modeled using a simple shear-lag approach [12]. At higher levels of strain failure of the graphene/polymer interface appeared to occur [10]. Since the size of the Raman laser spot employed was only the order of 1 μm compared to flake dimension in excess of 100 μm^2, it was also possible to map the strain distribution over a relatively large flake during deformation [11]. It was found that at relatively low strains (≤ 0.4%), the strain distribution in the flake was relatively uniform, with the strain in the flake being the same as the strain in the matrix. At higher strains, however, the strain distribution became non-uniform due probably to fragmentation of the polymer matrix [11]. Our research upon Raman band shifts in these model graphene nanocomposites has therefore demonstrated clearly that individual exfoliated flakes of graphene have the capability of reinforcing a polymer matrix. It appears that the approach can also be extended to higher loadings of graphene from other sources since there are recent reports of significant shifts of the Raman G band being obtained during the deformation of a nanocomposite consisting of ~ 0.1% of graphene platelets, obtained by the thermal reduction of graphene oxide, in a poly(dimethyl siloxane) matrix [13]. As stress transfer to monolayer graphene is now relatively well understood, the aim of this present study was to evaluate and compare the levels of reinforcement in nanocomposites by exfoliated graphene flakes consisting of a different numbers of layers, paying particular attention to the behavior of bilayer, trilayer and many-layer graphene materials.

2 Materials and Methods

The specimens were prepared using 5 mm thick poly(methyl methacrylate) beams spin-coated with 300 nm of cured SU-8 epoxy resin as described elsewhere [10,11]. The graphene was produced by mechanical cleaving of graphite and deposited on the surface of the SU-8. For some beams a thin 300 nm layer of SU-8 was then spin-coated on top and cured so that the graphene remained visible when sandwiched between the two coated polymer layers. This method produced graphene with a range of different numbers of layers that were identified both optically and by using Raman spectroscopy [7]. The PMMA beams were deformed in 4-point bending up to 0.4% strain with the strain monitored using a strain gage attached to the beam surface. Well-defined Raman spectra could be obtained from the graphene with different numbers of layers, using either a low-power (< 1 mW at the sample) HeNe laser (1.96 eV) or near IR laser (1.58 eV) in Renishaw 1000 or 2000 spectrometers. The laser beam polarizations were always parallel to the tensile axis and the spot size of the laser beams on the sample was approximately 2 μm using a 50× objective lens. One uncoated beam was unloaded after initial measurements had been made and then coated with a layer of cured SU-8. The beam was reloaded initially up to 0.4% strain, and the deformation of the monolayer and bilayer graphene on same flake on the surface of the beam was again followed from the shift of the 2D (or G') Raman band. The beam was then unloaded and then reloaded to various other levels of strain and the shift of a trilayer region on the same flake and a many-layer graphene flake was also followed from the shift of the 2D (or G') Raman band. The strains in the graphene flake containing both monolayer and bilayer regions were mapped

fully at each strain level as well as in the unloaded state. Raman spectra were obtained at different strain levels through mapping over the graphene monolayer in steps of between 2 μm and 5 μm by moving the *x-y* stage of the microscope manually and checking the position of the laser spot on the specimen relative to the image of the monolayer on the screen of the microscope. The strain at each measurement point was determined from the position of the 2D Raman band using the calibrations in Figure 1 and strain maps of the bilayer were produced in the form of coloured *x-y* contour maps using the OriginPro 8.5 graph-plotting software package, which interpolates the strain between the measurement points. One-dimensional plots of the variation of strain across the flake were also plotted along the rows indicated in Figure 4, at different levels of matrix strain.

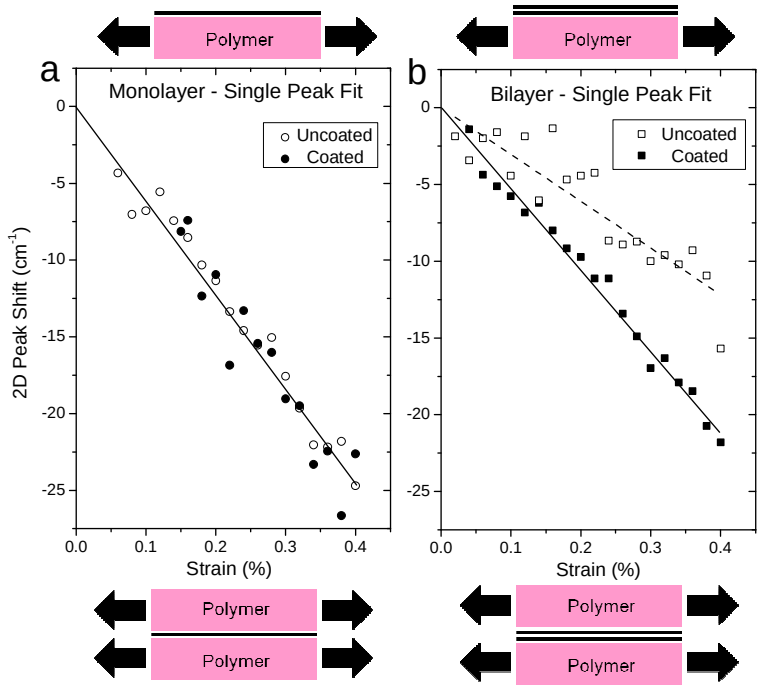

Figure 1. Shift with strain of 2D Raman band of the graphene fitted to a single peak during deformation upon the PMMA beam (laser excitation 633 nm). (a) A graphene monolayer deformed before and after coating with SU-8. (b) A graphene bilayer deformed before and after coating with SU-8. (Schematic diagrams of the deformation of the uncoated (above) and coated (below) graphene are also included).

3 Results and Discussion

Deformation of the graphene was undertaken by bending polymer beams on which flakes had been deposited. This leads to an axial strain in the graphene whereas the stress is somewhat biaxial in nature due to Poisson's contraction effects. Since all measurements were undertaken under similar conditions, all data are quoted in terms of graphene strain and only the relative bands shifts during deformation were considered. The shift of the 2D band with tensile strain for different monolayer and bilayer graphene flakes, deformed both before and after applying the SU-8 top-coat, is shown in Figure 1. The maximum strain in this case was 0.4% which is known to be below the level of strain at which debonding of the flakes or matrix polymer cracking can occur [11]. It can be seen from Figure 1a that the shift of the 2D Raman band for the graphene monolayer is -59 cm^{-1}/% strain and similar with and without the polymer top-coat. It is well established that the rate of shift per unit strain of the 2D Raman band for monolayer graphene depending upon the crystallographic orientation of the monolayer relative to the strain axis [14] and this value is within the range found by others, in both uncoated and coated specimens. In contrast, it is shown in Figure 1b that when the 2D Raman band is fitted to a single peak, the rate of shift per unit strain for an uncoated graphene bilayer (-31 cm^{-1}/% strain) is significantly less that of the same flake deformed after being coated (-53

cm^{-1}/% strain). The implications of this observation for the bilayer is that stress transfer between the polymer substrate and the graphene is relatively good, as has been found before [10], but that the efficiency of stress transfer between the lower and upper graphene layers is relatively poor. This is not an issue for the monolayer in Figure 1a where the presence of the top-coat makes no difference to the band shift rate. The band-shift data in Figure 1b are for the 2D band for the bilayer graphene fitted to a single peak. It is well established [7] that the 2D band for the bilayer material can be fitted to four peaks as shown in the Supporting Information. Details of this band are also shown in the Supporting Information before and after deformation for the specimen both uncoated and coated. It is found that the four peaks making up the band shift during deformation but remain otherwise unchanged (except for small relative intensity changes), demonstrating that the A-B Bernal stacking is maintained during the deformation of the specimen, in both the uncoated and coated states.

In order to gain a further insight into the behavior of flakes with different numbers of graphene layers the deformation of a single coated flake containing distinct regions of monolayer, bilayer and trilayer graphene was first investigated. An optical micrograph of the flake is given in Figure 2a along with a schematic diagram in Figure 2b showing the different regions in the micrograph determined from both thickness contrast and Raman spectra. The 2D Raman spectra obtained from the monolayer, bilayer and trilayer regions are shown in Figure 2c-e respectively. It can be seen that the monolayer 2D band comprises a single peak whereas the bilayer and trilayer 2D bands can be fitted to four and six sub-bands respectively [15]. In addition, a 2D band of a coated many-layer graphene flake is given for reference in Figure 2f. The band in this case is similar to that of graphite [15].

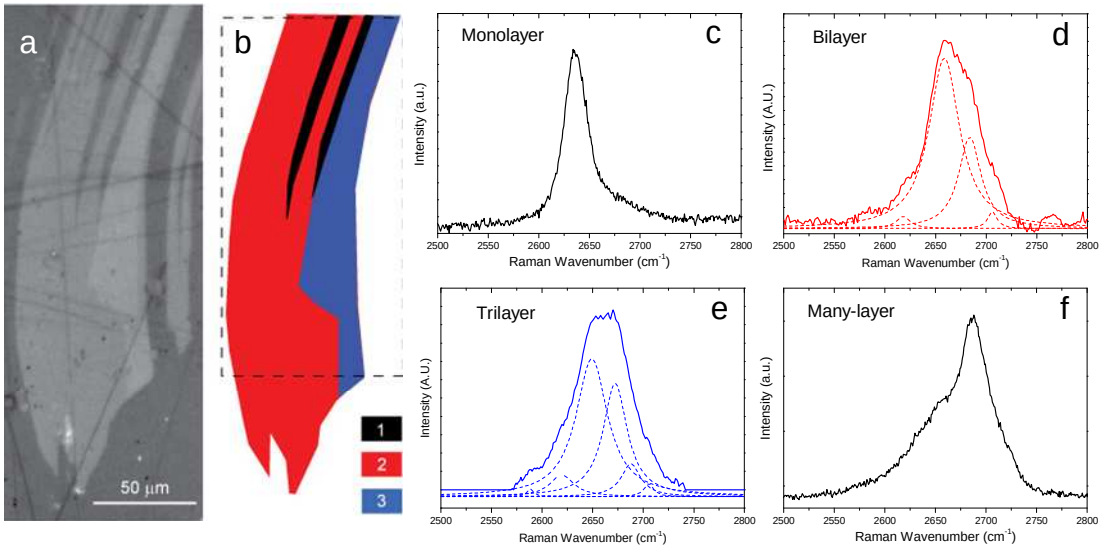

Figure 2. Graphene flake on a PMMA beam showing monolayer, bilayer and trilayer regions. (a) Optical micrograph. (b) Schematic diagram of the flake highlighting the different areas (the rectangle shows the area of the flake over which the strain was mapped). (c-f) Raman spectra of the 2D band part of the spectrum for the monolayer, bilayer (fitted to 4 peaks), trilayer regions (fitted to 6 peaks) and a multilayer graphene flake, elsewhere on the beam (laser excitation 633 nm).

Figure 3 shows how the deformation of the middle of adjacent monolayer, bilayer and trilayer regions of the flake in Figure 2 up to 0.4% strain was followed from the shifts of their 2D Raman bands. The advantage of doing this on the same flake is that it can be ensured that the orientation of the graphene is identical in each region (A-B Bernal stacking is confirmed from the forms of the 2D bands [15] in Figure 2c-f). The shift with strain of the four components of the bilayer graphene 2D band is shown in Figure 3a. The shift of the adjacent monolayer

region is shown for comparison. The 2D1B and 2D2B sub-bands (labeled) are relatively weak and therefore are somewhat scattered but it can be seen that the slope of the two strong components 2D1A and 2D2A, are similar to each other, (-53 and -55 cm^{-1}/% strain respectively) and also similar to the slope of the adjacent monolayer region (-52 cm^{-1}/% strain). The 2D band shifts with strain of the four different coated graphene structures is given in Figure 3b, with 2D band force fitted to a single Lorentzian peak in each, for comparison purposes. The many-layer graphene was from a different region of the specimen and the strain in trilayer was off-set since it was deformed after pre-loading of the beam to examine the behavior other regions and so a permanent set had developed. The 2D Raman band positions at a given strain are off-set from each other due to differences in the band structure of the different forms of graphene, as has been shown elsewhere [7,15]. It can also be seen that the slopes of the plots are similar for the monolayer and bilayer material (-52 and -53 cm^{-1}/% strain respectively) but somewhat lower for trilayer at -44 cm^{-1}/% strain. In contrast, the slope for the many-layer graphene is significantly lower at around -8 cm^{-1}/% strain.

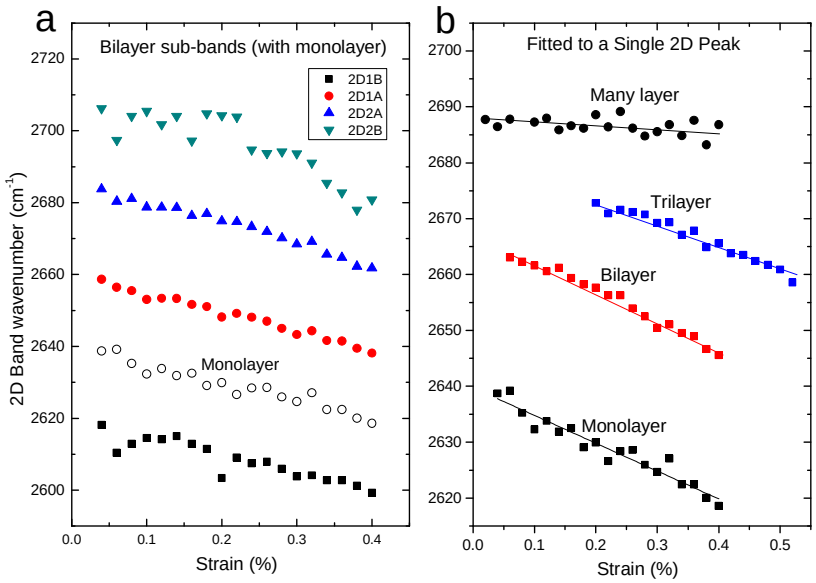

Figure 3. (a) Shift with strain of the four components of the 2D Raman band of the bilayer graphene shown on the specimen in the Figure 2 along with the shift of the 2D band in an adjacent monolayer region on the same flake (laser excitation 633 nm). (b) Shifts with strain of the 2D band for adjacent monolayer, bilayer and trilayers regions on the specimen in Figure 2, along with the shift with strain for the 2D band of a multilayer flake on the same specimen (all 2D bands were force fitted to a single Lorentzian peak).

Number of layers	Coating	$d\omega_{2D}/d\varepsilon$ (cm^{-1}/% strain)	Number of flakes studied
1	Uncoated	-48.8 ± 2.5	3
2	Uncoated	-38.9 ± 2.4	3
3	Uncoated	-32.4 ± 0.4	2
Many	Uncoated	-37.4 ± 8.2	3
Graphite	Uncoated	-3	1
1	Coated	-57.7 ± 7.8	4
2	Coated	-53.9 ± 2.9	4
3	Coated	-46.6 ± 9.0	6
Many	Coated	-40.2 ± 14.2	7
Graphite	Coated	0	2

Table 1. Measured 2D Raman band shift rates (with standard deviations) for the uncoated and coated graphene nanocomposite specimens described in the Supporting Information (laser excitation 785 nm). All bands were fitted to a single Lorentzian peak and the number of flakes on which the measurements were made is indicated.

Although the data shown in Figures 1 & 3 suggest that the 2D band shifts rates vary with the number of layers in the graphene and the presence or of absence a polymer top coat, there is always the possibility that such variations may be due to inhomogeneities or uneven stress transfer due to slippage [16]. Variations in the band shift behavior are also known to occur due differences in excitation wavelength, relative orientation of the graphene lattice to the straining direction and direction of laser polarization [9]. Because of this a systematic study was undertaken of the band shifts during deformation for more than 30 different graphene flakes on polymer beams in different orientations, consisting of different numbers of layers, both uncoated and with a polymer top coat. A different laser excitation was also employed (785 nm rather than 633 nm) and the data were carefully screened for evidence of slippage. Details of the relative 2D band shift rates with strain are summarized in Table 1.

For the uncoated specimens in Table 1, it can be seen that there is a decrease in the band shift rate for the flakes as the number of layers in increased from one to three. The shift rate data are more scattered for the multilayer flakes as is impossible to know the exact number of layers in such flakes. The shift rate for a graphite flake on the same uncoated specimen is also very low. In contrast the band shift rates are generally higher in the case of the coated specimen. The monolayer and bilayer flakes in the coated specimen have the same band shift rate within the limits of experimental error and the band shift rate then decreases for the three layer and multilayer flakes (again more scattered for the same reason as before). The shift rate for a graphite flake is again very low. The band shift behavior shown in Figures 1 & 3 is completely consistent with the comprehensive set of data in Table 1. Similarly Procter *et al*. [17] found that the band shift rate for (uncoated) bilayer graphene on the silicon substrate under pressure was slightly lower than that of the monolayer, whereas the shift rate of their "few-layer" graphene was only half that of the monolayer material. Although they suggested that that this lower rate for few-layer material could be due to poor adhesion with the substrate, the findings in Table 1 imply that it is more likely that this lower band shift rate is an inherent property of the few-layer material.

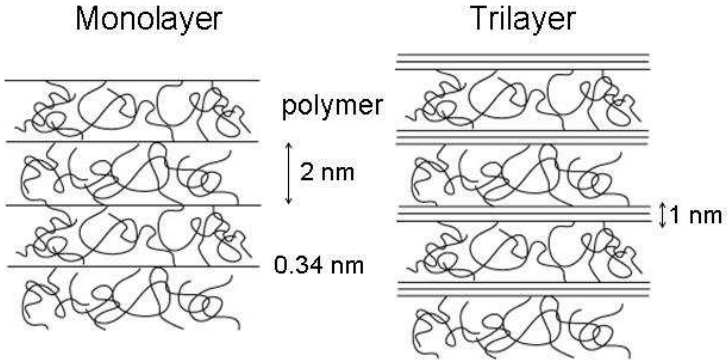

Figure 4. Schematic diagram of the microstructure of graphene-based nanocomposites based upon either monolayer or trilayer reinforcements. The interlayer spacing of the graphene is 0.34 nm and the effective thickness of the polymer coils is assumed to be to be around 2 nm.

It is well established that, to a first approximation, the band shift rates in Table 1 can be related to the efficiency of stress transfer to the graphene [10,11,18]. All the data were obtained from the middle of the flakes and by eliminating any data showing slippage at the graphene-polymer interface. Differences with respect to the monolayer will therefore principally be a result of the efficiency of stress transfer between the different graphene layers (the effect of different crystallographic orientations of the graphene will lead to only minor differences) [8]. This phenomenon is completely analogous to the efficiency of stress transfer between the different walls in multi-walled carbon nanotubes (MWNTs) analyzed by

Zalamea, Kim and Pipes [19]. They introduced a parameter k_i that characterizes the efficiency of stress transfer; for perfect transfer between the walls, $k_i = 1$ and for no stress transfer, $k_i = 0$. This analysis has been used to successfully model [20] stress transfer between the outer and inner walls of double-walled carbon nanotubes (DWNTs), made by the pea-pod route [21], in a nanocomposite. It is shown in the Supporting Information that it is relatively easy to adapt this theory to model stress transfer between the layers of multi-layer graphene.

At this stage it is worth considering the relative advantage of using bilayer graphene compared with the monolayer material. If we take two monolayer flakes dispersed well in a polymer matrix, the closest separation they can have will be of the order of the dimension of a polymer coil, i.e. at least several nm [22]. In contrast the separation between the two atomic layers in bilayer graphene is only around 0.34 nm and so it will be easier to achieve higher loadings of the bilayer material in a polymer nanocomposite, leading to an improvement in reinforcement ability by up to a factor of two over the monolayer material. It is also possible to determine the optimum number of layers need in the graphene flakes for the best levels of reinforcement in polymer-based nanocomposites. It was pointed out above that the effective Young's modulus of monolayer and bilayer graphene is similar and that it decreases as the number of layers decreases. In high volume fraction nanocomposites it will be necessary to accommodate the polymer coils between the graphene flake and the coil dimensions will limit the separation of the flakes as shown schematically in Figure 4. Similar issues have been considered by Klein and Luckham [23] for polymer solutions between parallel mica platelets and also by de Gennes [24]. The minimum separation of the graphene flakes will depend upon the type of polymer (i.e. it chemical structure and molecular conformation) and its interaction with the graphene [25]. It is unlikely that the minimum separation will be less than 1 nm and more likely that it will be several nm. The separation of the layers in multilayer graphene, on the other hand, is of the order of 0.34 nm.

4 Conclusions

It has been demonstrated that although there is good stress transfer between a polymer matrix and monolayer graphene, monolayer graphene is not the optimum material to use for reinforcement in graphene-based polymer nanocomposites. There is also good stress transfer from the polymer matrix to the bilayer material and no slippage between the layers when it is fully encapsulated in a polymer matrix. Less efficient stress transfer has been found for trilayer and many-layer graphene due to slippage between the internal graphene layers, indicating that such materials will have a lower effective Young's modulus than either monolayer or bilayer graphene in polymer-based nanocomposites. However, since the inter-layer spacing in multi-layer graphene is only 0.34 nm and so an order of magnitude less than the dimensions of polymer coils, higher volume fractions of graphene can be obtained for multi-layer material. There is therefore a balance to be struck in the design of graphene-based nanocomposites between the ability to achieve higher loadings of reinforcement and the reduction in effective Young's modulus of the reinforcement, as the number of layers in the graphene is increased.

References

[1] Geim, A. K.; Novoselov, K. S. The Rise of Graphene. *Nature Mater*., 2007, **6**, 183-190.
[2] Novoselov, K. S. Nobel Lecture: Graphene: Materials in the Flatland, *Reviews of Modern Physics*, 2011, **83**, 837-849.
[3] Geim, A. K. Nobel Lecture: Random Walk to Graphene. *Reviews of Modern Physics*, 2011, **83**, 851-862.

[4] Novoselov, K. S.; Geim, A. K.; Morozov, S. V.; Jiang, D.; Zhang, Y.; Dubonos S. V.; Grigorieva, I. V.; Firsov, A. A. Electric Field Effect in Atomically Thin Carbon Films. *Science*, 2004, **306**, 666 -669.
[5] Novoselov, K. S.; Geim, A. K.; Morozov, S. V.; Jiang, D.; Katsnelson, M. I.; Grigorieva, I. V.; Dubonos, S. V.; Firsov, A. A. Two-dimensional Gas of Massless Dirac Fermions in Graphene. *Nature*, 2005, **438**, 197-200.
[6] Lee, C.; Wei, X. D.; Kysar J. W.; Hone J. Measurement of the Elastic Properties and Intrinsic Strength of Monolayer Graphene. *Science*, 2008, **321**, 385-388.
[7] Ferrari, A. C.; Meyer, J. C.; Scardaci, V.; Casiraghi, C.; Lazzeri, M.; Mauri, F.; Piscanec, S.; Jiang, D.; Novoselov, K. S.; Roth, S.; Geim, A. K. Raman Spectrum of Graphene and Graphene Layers. *Phys. Rev. Lett.*, 2006, **97**, 187401.
[8] Huang, M. Y.; Yan, H.; Chen, C. Y.; Song, D. H.; Heinz, T. F.; Hone, J. Phonon Softening and Crystallographic Orientation of Strained Graphene Studied by Raman Spectroscopy. *Proc. Natl. Acad. Sci.*, 2009, **106**, 7304-7308.
[9] Mohiuddin, T. M. G.; Lombardo, A.; Nair, R. R.; Bonetti, A.; Savini, G.; Jalil, R.; Bonini, N.; Basko, D. M.; Galiotis, C.; Marzari, N.; *et al*. Uniaxial Strain in Graphene by Raman spectroscopy: G Peak Splitting, Gruneisen Parameters, and Sample Orientation. *Phys. Rev. B*, 2009, **79**, 205433.
[10] Gong, L.; Kinloch, I. A.; Young, R. J.; Riaz, I.; Jalil, R.; Novoselov, K. S. Interfacial Stress Transfer in a Graphene Monolayer Nanocomposite. *Adv. Mater*., 2010, **22**, 2694-2697.
[11] Young, R. J.; Gong, L.; Kinloch, I. A.; Riaz, I.; Jalil R.; Novoselov, K. S., Strain Mapping in a Graphene Monolayer Nanocomposite, *ACS Nano*, 2011, **5**, 3079-3084.
[12] Kelly, A.; Macmillan, N. H. *Strong Solids*, 1986, 3rd Edition, Clarendon Press: Oxford.
[13] Srivastava, I.; Mehta, R. J.; Yu, Z.-Z.; Schadler, J; Koratkar, N., Raman Study of Interfacial Load Transfer in Graphene Nanocomposites, *Appl. Phys. Lett*., 2011, **98**, 063102.
[14] Frank, O.; Mohr, M.; Maultzsch, J.; Thomsen, C.; Riaz, I.; Jalil, R.; Novoselov, K. S.; Tsoukleri, G.; Parthenios, J.; Papagelis, K.; et al. Raman 2D-Band Splitting in Graphene: Theory and Experiment, ACS Nano, 2011, **5**, 2231-2239.
[15] Malard, L. M.; Pimenta, M. A.; Dresselhaus, G.; Dresselhaus, M. S. Raman Spectroscopy in Graphene. *Phys. Rep*., 2009, **473**, 51-87.
[16] Frank O.; Bouša M.; Riaz I.; Jalil R.; Novoselov K. S.; Tsoukleri G.; Parthenios J.; Kavan L.; Papagelis K.; Galiotis C. Phonon and Structural Changes in Deformed Bernal Stacked Bilayer Graphene. *Nano Lett*., 2012, dx.doi.org/10.1021/nl203565p
[17] Proctor, J. E.; Gregoryanz, E.; Novoselov, K. S.; Lotya, M.; Coleman, J. N.; Halsall, M. P. High-Pressure Raman Spectroscopy of Graphene. *Phys. Rev. B*, 2009, **80**, 073408.
[18] Frank, O.; Tsoukleri, G.; Riaz, I.; Papagelis, K.; Parthenios, J.; Ferrari, A. C.; Geim, A. K.; Novoselov, K. S.; Galiotis, C. Development of a Universal Stress Sensor for Graphene and Carbon Fibres, *Nature Comm.*, 2011, **2**, 255.
[19] Zalamea, L.; Kim, H.; Pipes, R. B., Stress Transfer in Multi-Walled Carbon Nanotubes. *Comp. Sci. Tech.*, 2007, **67**, 3425-3433.
[20] Cui, S.; Kinloch, I. A.; Young, R. J.; Noe, L.; Monthioux, M., The Effect of Stress Transfer Within Double-Walled Carbon Nanotubes Upon Their Ability to Reinforce Composites, *Adv. Mater.*, 2009, **21**, 3591-3596.
[21] Ding, F.; Xu, Z. W.; Yakobson, B. I.; Young, R. J.; Kinloch, I. A.; Cui, S.; Deng, L. B.; Puech, P; Monthioux, M., Formation Mechanism of Peapod-Derived Double-Walled Carbon Nanotubes. *Phys. Rev. B*, 2010, **82**, 041403
[22] Young, R. J.; Lovell, P.A. Introduction to Polymers, 2011, 3rd Edition, CRC Press, Boca Baton.
[23] Klein, J.; Luckham, P. F. Long-Range Attractive Forces between Two Mica Surfaces in an Aqueous Solution. *Nature*, 1984, **308**, 836-837.
[24] de Gennes, P. G. Polymers at an Interface: A Simplified View. *Adv. Polym. Sci*, 1987, **27**, 189-209.
[25] Gong, L.; Young, R. J.; Kinloch, I.A.; Riaz, I.; Jalil, R.; Novoselov, K.S. Optimizing the Reinforcement of Polymer-Based Nanocomposites by Graphene, *ACS Nano*, 2012, **6**, 2086-2095.